Liquid Crystals
Publication details, including instructions for authors and subscription information:
http://www.informaworld.com/smpp/title~content=t713926090

Nematic liquid crystal in contact with periodically patterned surfaces

S. Kondrat[a]; A. Poniewierski[a]; L. Harnau[bc]
[a] Institute of Physical Chemistry, Polish Academy of Sciences, Kasprzaka 44/52, 01-224 Warsaw, Poland [b] Max-Planck-Institut für Metallforschung, Heisenbergstr. 3, D-70569 Stuttgart, Germany [c] Institut für Theoretische und Angewandte Physik, Universität Stuttgart, Pfaffenwaldring 57, D-70569 Stuttgart, Germany

To cite this Article Kondrat, S. , Poniewierski, A. and Harnau, L.(2005) 'Nematic liquid crystal in contact with periodically patterned surfaces', Liquid Crystals, 32: 1, 95 — 105
To link to this Article: DOI: 10.1080/02678290512331324039
URL: http://dx.doi.org/10.1080/02678290512331324039

Liquid Crystals, Vol. 32, No. 1, January 2005, 95–105

Nematic liquid crystal in contact with periodically patterned surfaces

S. KONDRAT, A. PONIEWIERSKI* and L. HARNAU†‡

Institute of Physical Chemistry, Polish Academy of Sciences, Kasprzaka 44/52, 01-224 Warsaw, Poland
†Max-Planck-Institut für Metallforschung, Heisenbergstr. 3, D-70569 Stuttgart, Germany
‡Institut für Theoretische und Angewandte Physik, Universität Stuttgart, Pfaffenwaldring 57, D-70569 Stuttgart, Germany

(*Received 6 November 2003; in final form 13 August 2004; accepted 26 August 2004*)

Nematic liquid crystals confined between two different substrates, possessing alternating stripe patterns of planar and homeotropic anchoring, are studied within the Frank–Oseen theory, in which the anchoring energy function is given by the Rapini–Papoular expression. By numerical minimization of the free energy we determine phase transitions between uniform and distorted nematic textures. The calculations reveal that these phase transitions can be triggered by changing the shift of the stripe patterns with respect to each other. A hybrid nematic cell model together with an effective anchoring strength can be used to describe the phase behaviour for sample thicknesses larger than the periodicity of the stripe pattern. Rich phase behaviour is predicted for the case of a generalized expression for the surface free energy.

1. Introduction

Alignment of nematic liquid crystals (NLCs) induced by surfaces is interesting both from practical and fundamental points of view. The presence of a limiting surface breaks the rotational symmetry of the liquid by imposing a preferred orientation on the adjacent molecules. Thus, in the absence of external fields or other surfaces, the average molecular orientation $\hat{\mathbf{n}}$ (the director) adopts in the bulk a particular orientation called the easy axis or the anchoring direction [1, 2]. This phenomenon is known as anchoring. If $\hat{\mathbf{n}}$ at the surfaces changes when a bulk deformation is imposed the anchoring is referred to as weak, otherwise it is termed strong. If there is only one orientation of $\hat{\mathbf{n}}$ favoured by the NLC–surface interaction, anchoring is said to be monostable; if there is a degenerate set of such orientations it is called multistable. In particular, bistable anchoring has received attention recently, because of potential applications in liquid crystal (LC) display devices [2–10]. One of the means for obtaining bistable anchoring is a SiO film evaporated under oblique incidence [3]. Recently it has been demonstrated that periodic surfaces can also be used to obtain bistable nematic devices and the role of surface grating structures [9] and defects near the surface [10] has been studied.

It is well known that surface inhomogeneities, such as surface roughness [11, 12] or patterns of different surface composition [13–16], influence anchoring of NLCs. These inhomogeneities are usually in a nanometer range, implying that the surface is macroscopically homogeneous because the thickness of the boundary layer, where the director field is non-uniform, is comparable to the fundamental wavelength of the surface pattern [13]. More recently it has been shown that patterned surfaces with a fundamental wavelength in the micrometer range are also of great interest [17–21]. For example, a pattern of different anchoring regions can be obtained by means of self-assembled monolayers on both flat and curved surfaces [17]. It has been shown that the alignment of LC molecules can be determined just by the pattern of boundary lines between different regions and the LC elasticity [18]. Adjacent regions of planar and homeotropic anchoring have been created by micro-contact printed polar and apolar thiols, respectively, on an obliquely evaporated ultra-thin gold layer [20].

In this paper we study a NLC in contact with flat periodically patterned surfaces. The pattern is formed by stripes of alternating homeotropic and planar anchoring. The NLC is described within the Frank–Oseen theory [22], and the anchoring energy function is

*Corresponding author. Email: apon@meta.ichf.edu.pl

Liquid Crystals
ISSN 0267-8292 print/ISSN 1366-5855 online © 2005 Taylor & Francis Ltd
http://www.tandf.co.uk/journals
DOI: 10.1080/02678290512331324039

given by the Rapini–Papoular expression [23]. Our model is similar to the one introduced by Barbero *et al.* [14]. In previous studies we have applied this model to a NLC in contact with a single periodic substrate [24] or placed between two identical periodic substrates [25]. We have studied the influence of the cell thickness D on the nematic textures and the NLC mediated interaction between the substrates [25]. Here we generalize the model to allow for different stripe patterns on each surface, as well as for a shift of one pattern with respect to the other.

One of the objectives of the present work is to study the anchoring energy function for periodically patterned substrates. If the distance from a single substrate is large in comparison with the periodicity of the surface structure p, the texture of the NLC is uniform. Thus, on scales large compared with p the substrate is effectively homogeneous [13, 14]. The anchoring properties of such an effective homogeneous substrate are usually different from the local anchoring properties of the constituent regions. Using the Rapini–Papoular expression [23] for the local anchoring on each stripe, we show that the anchoring on the effective homogeneous substrate obtained from our model is governed by an anchoring energy function that deviates from the Rapini–Papoular form. We draw this conclusion from studies of a hybrid nematic cell (HNC) with two patterned surfaces of competing effective anchoring.

Section 2 presents phase diagrams of a NLC confined by two flat substrates possessing an alternating stripe pattern of planar and homeotropic anchoring. The effective anchoring strength of a single substrate, as well as the phase behaviour of the HNC in the case of a generalized form of the anchoring energy function, are investigated in § 3. Our results are summarized in § 4.

2. NLC between flat periodic substrates

We consider a NLC confined by two parallel flat substrates at $z=0$ and $z=D$, where the z axis is normal to the substrates. As figure 1 illustrates, both substrates are characterized by stripe patterns of periodicity p along the x axis. More specifically, in this study the surfaces of the substrates consist of alternating stripes of homeotropic (H) and homogeneous planar (P) (along the x direction) anchoring. The system is translationally invariant in the y direction. It proves convenient to assign an index i to the width $p_i^{(\alpha)}$ and the anchoring strength coefficient $w_i^{(\alpha)} > 0$ of each stripe, such that $i=1$ corresponds to stripes of type H and $i=2$ corresponds to stripes of type P. The two substrates at $z=0$ and $z=D$ are designated by $\alpha=0$ and $\alpha=D$, respectively. Note that $p_1^{(\alpha)}+p_2^{(\alpha)}=p$. The shift of the stripe patterns

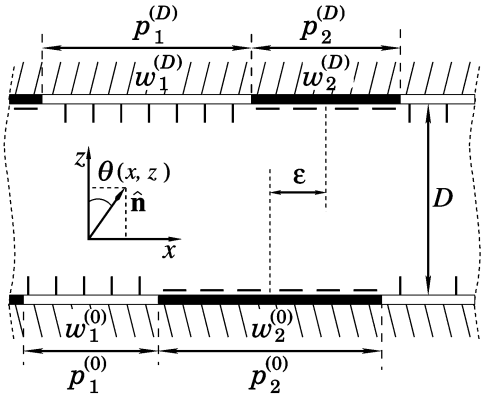

Figure 1. The system under consideration consists of a nematic liquid crystal (NLC) confined between two substrates at $z=0$ and $z=D$ with alternating stripe patterns of homeotropic anchoring (white bars) and homogeneous planar anchoring (black bars). The stripes are oriented along the y axis perpendicular to the plane of the figure, and the relative shift of the stripe patterns is denoted by ε. The widths of the stripes and the anchoring strength coefficients are designated by $p_i^{(\alpha)}$ and $w_i^{(\alpha)}$, respectively.

on the two substrates with respect to each other is denoted ε (see figure 1).

The free energy of the confined NLC is given by

$$F=\frac{K}{2}\int_0^D \mathrm{d}z\int_0^p \mathrm{d}x[\nabla\theta(x,z)]^2+\frac{1}{2}\int_0^p \mathrm{d}x\left[w_0(x)\sin^2\theta_0(x)+w_D(x)\sin^2\theta_D(x)\right] \tag{1}$$

where $\theta_0(x)=\theta(x, 0)$ and $\theta_D(x)=\theta(x, D)$. The first term on the right hand side is the distortion free energy (F_d) [1, 22] within the one-constant approximation and the second term is the surface free energy (F_s) adopting the Rapini–Papoular form [23]. The anchoring strengths are specified by periodic step functions: $w_\alpha(x)=w_1^{(\alpha)}$ and $w_\alpha(x)=-w_2^{(\alpha)}$ for values of x on the H-stripes and P-stripes, respectively. A shift of one stripe pattern with respect to the one on the other substrate is taken into account in terms of $w_\alpha(x)$, and $\varepsilon=0$ means that the midlines of corresponding H-stripes and P-stripes at $z=0$ and $z=D$ have the same x coordinates (see figure 1). For obvious symmetry reasons it is sufficient to consider only $0<\varepsilon<p/2$. It proves convenient to introduce extrapolation lengths $b_i^{(\alpha)}=K\big/w_i^{(\alpha)}$[1].

Minimization of F with respect to $\theta(x, z)$ leads to the Laplace equation:

$$\nabla^2\theta(x,z)=0 \tag{2}$$

with two boundary conditions:

$$K\frac{\partial\theta(x,z)}{\partial z}\bigg|_{z=0} = \frac{1}{2}w_0(x)\sin[2\theta_0(x)]$$
$$K\frac{\partial\theta(x,z)}{\partial z}\bigg|_{z=D} = -\frac{1}{2}w_D(x)\sin[2\theta_D(x)] \quad (3)$$

There are three possible solutions of Equations (2) and (3): $\theta(x, z)=0$, $\theta(x, z)=\pi/2$, and $\theta(x, z)\neq const$. The first two solutions correspond to uniform homeotropic and planar textures denoted by U_0 and $U_{\pi/2}$, respectively. The third solution describes a non-uniform texture designated NT. This texture exhibits an average tilt of the director with respect to the normal (averaged over a period of the structure).

In the case of a single substrate (semi-infinite system) the second boundary condition in expression (3) becomes $\lim_{z\to\infty}\partial\theta/\partial z=0$ [24]. A periodic substrate induces an anchoring direction, which we call *the effective anchoring direction* (denoted $\theta_a^{(eff)}$) in order to distinguish from the local anchoring directions of different regions in the surface pattern. In the absence of external fields or competing surfaces the director $\hat{\mathbf{n}}$ adopts the orientation $\theta_a^{(eff)}$ when the distance from the substrate is large compared with the period of the pattern. Note that as long as the substrate is assumed to be flat the NT type always corresponds to effective anchoring directions $0 < \theta_a^{(eff)} < \pi/2$, hence, NT also means *a non-uniform tilted texture*. In the case of two substrates the NT type can also mean that the average tilt changes throughout the sample, for instance in a hybrid nematic cell.

Returning to textures induced by a single substrate, one could argue that the fact that $\theta(x, z)\to 0$ far from the surface, hence $\theta_a^{(eff)}=0$ by definition, does not necessarily imply that $\theta(x, z)=0$ everywhere. A hypothetical texture that would be homeotropic (far from the substrate) but not identical with the U_0 texture could, in principle, exist. We stress, however, that it does not occur in our simple model (at least we failed to find it), which means that $\theta_a^{(eff)}=0$ exclusively for the U_0 texture. Similarly, $\theta_a^{(eff)}=\pi/2$ exclusively for the $U_{\pi/2}$ texture. On the other hand, another type of the surface pattern or the surface free energy can lead to a homeotropic (or planar) alignment far from the substrate, accompanied by a non-uniform director field in the surface region. We shall return to this point in § 3.3. In particular, the inclusion of surface roughness could lead to such an effect but this is beyond the scope of the present work.

Instead of solving equation (2) with non-linear boundary conditions (3) it is convenient to perform the minimization of F in two steps. First a general solution of the Laplace equation is obtained in terms of arbitrary boundary functions $\theta_0(x)$ and $\theta_D(x)$, which leads to the functional $F[\theta_0, \theta_D]$. In the second step this functional is minimized with respect to the boundary functions. Since the second minimization has to be performed numerically the free energy functional is discretized as is shown in the appendix.

In figures 2 (*a*) and 2 (*b*) we present phase diagrams (in the (ε/p, D/p) plane) of a NLC confined by two identically patterned substrates ($b_i^{(0)}=b_i^{(D)}=b_i$ and $p_i^{(0)}=p_i^{(D)}=p_i$). The stripe widths are equal but the strength of homeotropic anchoring is larger than the strength of planar anchoring ($b_1<b_2$). Therefore the phase diagrams do not involve the $U_{\pi/2}$ texture. Upon decreasing b_2 the phase diagrams shown in figures 2 (*a*) and 2 (*b*) differ qualitatively, and it is worthwhile to distinguish the following cases.

(i) Figure 2 (*a*): At large distances D the U_0 texture is stable independent of the relative shift of the stripe patterns. This implies that each substrate separately favours the U_0 texture. The value of D at the second order U_0–NT transition decreases upon increasing ε. In the limit $\varepsilon\to p/2$ no non-uniform texture is found because distortions of $\hat{\mathbf{n}}$ are energetically unfavourable in the presence of the competing anchoring conditions on the corresponding lower and upper stripes.

(ii) Figure 2 (*b*): Decreasing b_2, as compared with figure 2 (*a*), leads to a non-uniform texture at large distances [24]. The U_0 texture is found to be stable only if $\varepsilon_0<\varepsilon<p/2$, where ε_0 depends on the values of the parameters b_1, b_2 and p_1/p. Phase transitions between the U_0 texture and a non-uniform texture occur at two different values of D. In both cases the transition is continuous. The first transition, at larger values of D, takes place because variations of $\hat{\mathbf{n}}$ in the z direction become energetically too costly if D decreases, reminiscent of the HNC behaviour discussed later. The second transition occurs when the substrates are close to each other. Below the transition the texture is characterized by extended regions of almost uniform homeotropic and planar alignment which are separated by non-uniform regions.

Figure 3 displays an alternative representation of the phase diagram in the (p/b_2, D/p) plane for various values of ε and a fixed value of p/b_1. The figure illustrates that the location of the U_0–NT transition as a function of p/b_2 is practically independent of ε for $D>p$. Moreover a reentrant phenomenon (NT–U_0–NT) is apparent for intermediate values of ε.

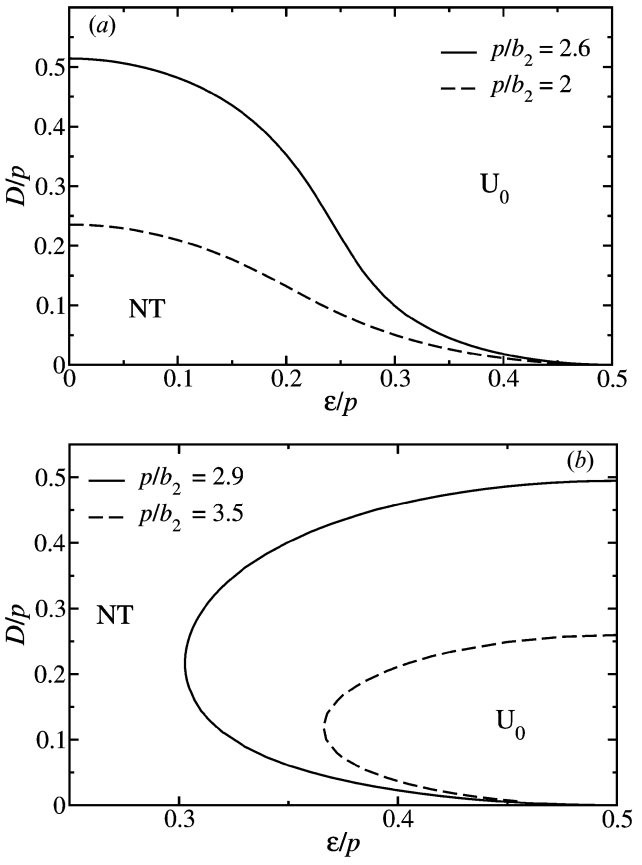

Figure 2. Phase diagrams of a NLC confined by two identical flat substrates with alternating stripe pattern of planar and homeotropic anchoring ($p_1^{(0)} = p_1^{(D)} = p/2$) as a function of the shift ε and the substrate separation D for four values of the strength of homeotropic anchoring $b_2 \equiv b_2^{(0)} = b_2^{(D)}$. The strength of planar anchoring is kept fixed at $b_1 \equiv b_1^{(0)} = b_1^{(D)} = p/10$. In the limit $D \to \infty$ the uniform homeotropic (U_0) and non-uniform (NT) texture is stable in (*a*) and (*b*), respectively.

We have also studied the case of different stripe patterns such that the lower substrate favours either the $U_{\pi/2}$ texture or a NT, whereas the upper substrate favours the U_0 texture. The anchoring strength of the H-stripes on the upper substrate is chosen to be stronger than that on the lower substrate. The results are shown in figures 4 (*a*) and 4 (*b*). Again we observe two U_0–NT transitions. The transition at the larger value of D can be explained in terms of a HNC with two effective homogeneous substrates (see § 3.2 for the details). As is apparent from the figures this approximation can be used for substrate separations D larger than the periodicity p. For smaller values of D the substrate inhomogeneities become important, resulting in the second U_0–NT transition. With a suitable choice of model parameters this second transition occurs for

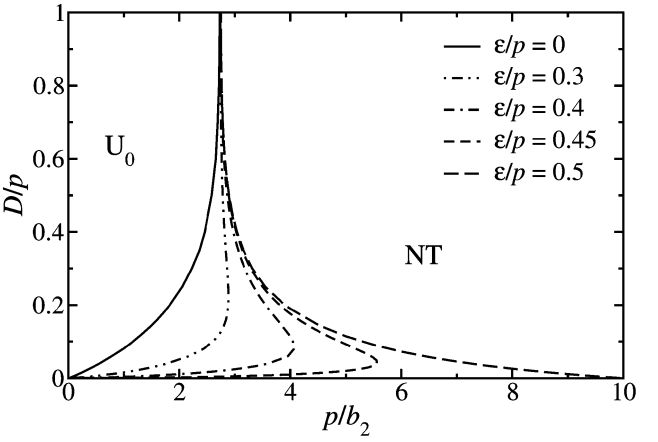

Figure 3. Phase diagram of a confined NLC, corresponding to figure 2, in the (p/b_2, D/p) plane for various values of ε.

arbitrary values of ε. We emphasize that the U_0 phase can also be stable in the case when the lower substrate induces a tilted nematic director $\hat{\mathbf{n}}$, see figure 4 (*b*). This cannot be explained by the Rapini–Papoular approximation [23] for the effective anchoring energy function. We return to this point in the next section.

3. Effective anchoring on a periodically patterned substrate

3.1. *Effective anchoring strength*

Let us consider a single substrate and a NLC in contact with it. When the distance from the substrate is much larger than the periodicity of the surface structure, the NLC is practically uniform and the orientation of $\hat{\mathbf{n}}$ in the bulk is given by the effective anchoring direction $\theta_a^{(\mathrm{eff})}$. It is of some interest to determine the strength of the effective anchoring and its relationship to the local anchoring strength coefficients w_1 and w_2. A possible approach to this problem is to place at some distance from the substrate a strongly anchoring wall with an anchoring direction different from the effective anchoring direction of the substrate. By studying the asymptotic behaviour of the free energy as a function of the wall separation it is possible to extract the effective extrapolation length.

A more straightforward method, which does not explicitly involve another surface, is based on a linearized equation for the director, in which the linearization is around the equilibrium solution [26]. Both methods are expected to give the same results [27], which we have verified for our model. We now describe briefly only the second method.

Let us assume that for a semi-infinite system ($D \to \infty$) we know the solution of equation (2), denoted as $\theta^{(\infty)}(x, z)$, which satisfies boundary condition (3) at $z = 0$. In the

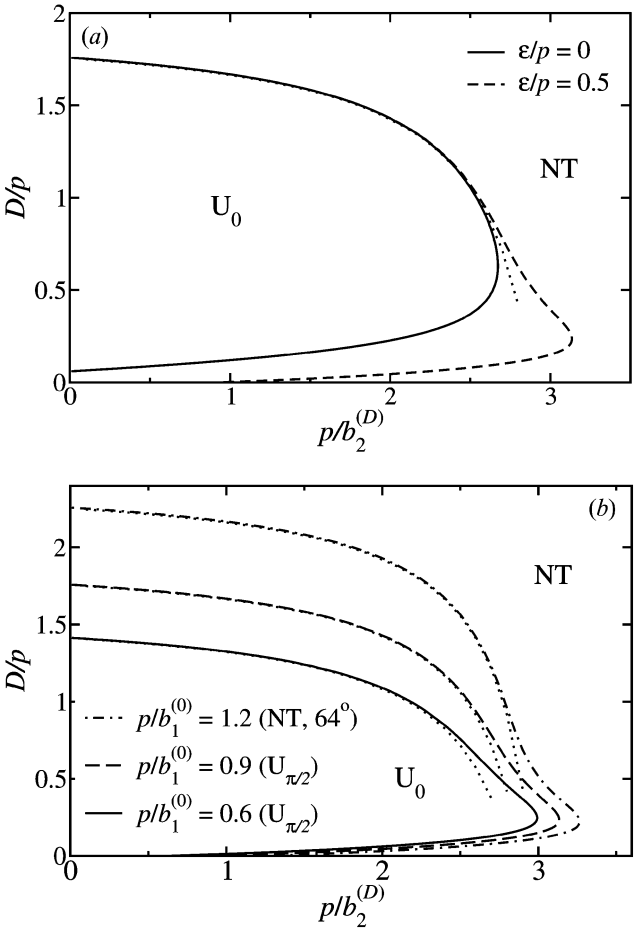

Figure 4. Phase diagrams of a NLC confined by two different flat substrates with alternating stripe patterns of planar and homeotropic anchoring ($p_1^{(0)}=p_1^{(D)}=p/2$) as a function of the extrapolation length of the planar anchoring stripes on the upper substrate, $b_2^{(D)}$, and the substrate separation D. The lower substrate favours the $U_{\pi/2}$ texture in (*a*), and the NT as well as the $U_{\pi/2}$ texture in (*b*), whereas the upper substrate favours the U_0 texture (for $p/b_2^{(D)} \lesssim 3.2$). The values of the remaining model parameters are given by: $p/b_1^{(0)}=0.9$, $p/b_2^{(0)}=1.5, p/b_1^{(D)}=20$ in (*a*), and $p/b_2^{(0)}=1.5, p/b_1^{(D)}=20$, $\varepsilon=p/2$ in (*b*). The dotted curves have been obtained from asymptotic formula (8) (see text).

absence of other surfaces or external fields, $\theta^{(\infty)}(x, z)$ approaches the bulk value $\theta_a^{(\text{eff})}$ exponentially as a function of the distance from the wall. Then we consider an external strain that deviates the director from $\theta_a^{(\text{eff})}$ far from the substrate. Thus, the director should be a linear function of z for large values of z and the new solution of equation (2) reads

$$\theta(x, z)=\theta^{(\infty)}(x, z)+\delta\theta(x, z)= \theta^{(\infty)}(x, z)+C[z+\psi(x, z)] \quad (4)$$

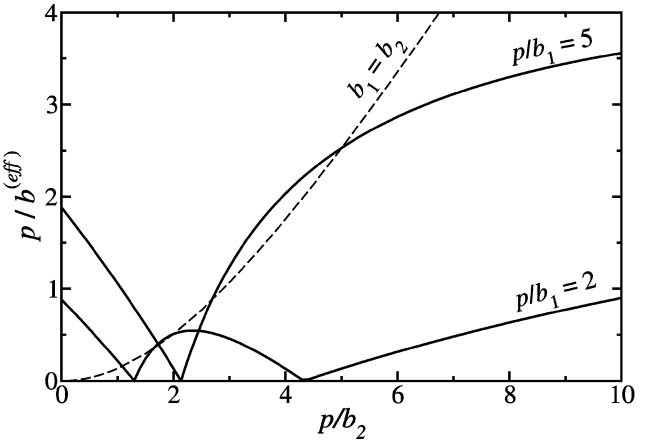

Figure 5. Strength of effective anchoring $p/b^{(\text{eff})}$ as a function of p/b_2 for a single substrate possessing an alternating stripe pattern of planar and homeotropic anchoring. The widths of the stripes are equal. U_0–NT or $U_{\pi/2}$–NT phase transitions correspond to $p/b^{(\text{eff})}=0$.

where C is a constant and $\nabla^2\psi=0$. In the case of a homogeneous substrate $\theta(z)\sim C(z+b)$ for large z, where b is by definition the extrapolation length, which characterizes the strength of anchoring [1, 26]. If the strain is applied to a NLC in contact with a patterned substrate, the director field close to the substrate must be non-uniform, even if the unperturbed texture was uniform. The effect of the strain is described by $\psi(x, z)$. To obtain the boundary condition for $\psi(x, z)$ at $z=0$ we substitute equation (4) into the first equation in (3). Then, using the fact that C can be made arbitrarily small, we linearize the right hand side with respect to C around $\theta_0^{(\infty)}(x)=\theta^{(\infty)}(x, 0)$. This yields

$$K\left(1+\left.\frac{\partial\psi(x, z)}{\partial z}\right|_{z=0}\right)=w_0(x)\cos\left[2\theta_0^{(\infty)}(x)\right]\psi(x, 0) \quad (5)$$

and the second boundary condition, at $z=\infty$, is given by $\partial\psi/\partial z=0$. Since $\psi(x, z)$ tends exponentially to a constant, for $z\to\infty$, θ has the same asymptotic form as for homogeneous substrates, i.e. $\theta(x, z)\sim C(z+b^{(\text{eff})})$, for large z. The effective extrapolation length, defined as $b^{(\text{eff})}=\lim_{z\to\infty}\psi(x, z)$, characterizes the patterned substrate as a whole and it should be distinguished from the local extrapolation lengths of the homeotropic and planar regions. To find $b^{(\text{eff})}$ we solve the Laplace equation with the two boundary conditions for $\psi(x, z)$ (see appendix). Having determined $b^{(\text{eff})}$ we can obtain the effective anchoring strength coefficient from the relationship $w^{(\text{eff})}=K/b^{(\text{eff})}$.

In figure 5 the ratio $p/b^{(\text{eff})}$, which is proportional to $w^{(\text{eff})}$, is plotted against p/b_2, for two values of p/b_1. For $p/b_1=2$, on increasing the ratio p/b_2 we first cross the U_0–NT phase bounadry and then the NT–$U_{\pi/2}$ phase

boundary. The points where $p/b^{(\mathrm{eff})}=0$ lie on the transition lines. For $p/b_1=5$, only the NT–$U_{\pi/2}$ phase boundary is crossed. As expected, $p/b^{(\mathrm{eff})}$ is always smaller than p/b_1 and p/b_2. Note that by varying the parameters of the model we are able to change $w^{(\mathrm{eff})}$ over a rather wide range. For comparison, we have also shown the case $b_1=b_2$, for which the unperturbed texture is always of the NT type.

3.2. *Hybrid nematic cell*

A HNC consists of a NLC placed between two substrates with competing anchoring conditions, usually homeotropic and planar. When the anchoring strength coefficients are different the nematic texture is uniform for small substrate separations and distorted for large separations. Thus, there is a critical thickness of the cell D_{cr}, at which a continuous phase transition occurs [28]. Application of equation (1) to homogeneous substrates leads to $D_{\mathrm{cr}}=|b_0-b_D|$, where $b_0=K/w_0$ and $b_D=K/w_D$ are the extrapolation lengths.

Here we study a HNC with two inhomogeneous substrates defined in § 2. First let us assume that each substrate, considered separately, favours a uniform nematic texture: planar at $z=0$ and homeotropic at $z=D$. The effective homeotropic anchoring is chosen to be stronger than the planar one. D_{cr} can then be determined by minimizing the free energy functional given by equation (1); see also equation (A6). However, if the transition is expected to occur at a large separation D, compared to the thickness of the interfacial regions ($\sim p$), we may consider effective homogeneous substrates [14]. This leads to a simplified expression for the free energy:

$$F\left(\bar{\theta}_0\,,\,\bar{\theta}_D\right)=\frac{K\left(\bar{\theta}_0-\bar{\theta}_D\right)^2}{2D}+\gamma_0\left(\bar{\theta}_0\right)+\gamma_D\left(\bar{\theta}_D\right) \quad (6)$$

where γ_α is the surface free energy associated with the NLC–substrate interface, considered as a function of an effective surface director $\bar{\theta}_\alpha$ [27]. In fact, we need only the dependence of γ_α on $\bar{\theta}_\alpha$ around its minimum and maximum. To study the stability limit of the homeotropic texture we expand γ_α around $\bar{\theta}_\alpha=0$, hence

$$F\approx\frac{K\left(\bar{\theta}_0-\bar{\theta}_D\right)^2}{2D}+\gamma_0(0)+\gamma_D(0)+\frac{1}{2}\gamma_0''(0)\,\bar{\theta}_0^2+\frac{1}{2}w_D^{(\mathrm{eff})}\,\bar{\theta}_D^2 \quad (7)$$

where $w_D^{(\mathrm{eff})}=\gamma_D''(0)>0$ is the effective anchoring strength coefficient for the homeotropic anchoring, obtained from the relation $w_D^{(\mathrm{eff})}=K\Big/b_D^{(\mathrm{eff})}$, and the effective extrapolation length $b_D^{(\mathrm{eff})}$ follows from equation (5).

To find $\gamma''_0(0)$ let us assume for a moment that the substrate at $z=D$ is homogeneous and exhibits strong homeotropic anchoring; hence $\theta(x, D)=0$. If the planar anchoring at $z=0$ is weak the nematic texture remains homeotropic for $D<D_{\mathrm{cr}}$, where $D\gtrsim p$. It is easy to see that D_{cr}, at which a non-uniform solution (satisfying the boundary condition at $z=D$) appears, can formally be obtained from equation (5) by choosing $\theta_0^{(\infty)}(x)=0$. The corresponding extrapolation length $\tilde{b}_0^{(\mathrm{eff})}$ is negative, hence, $D_{\mathrm{cr}}=-\tilde{b}_0^{(\mathrm{eff})}$. The second extrapolation length at $z=0$, $b_0^{(\mathrm{eff})}=K\big/\gamma_0''(\pi/2)>0$, corresponds to the minimum of $\gamma_0\left(\bar{\theta}_0\right)$. Note that in general $\left|\tilde{b}_0^{(\mathrm{eff})}\right|\neq b_0^{(\mathrm{eff})}$, which means that in our model $\gamma_0\left(\bar{\theta}_0\right)$ cannot be approximated by the Rapini–Papoular formula [23]. We do stress that although the Rapini–Papoular formula is most widely used to mimic the interaction of NLCs with substrates, more general forms of the anchoring energy function have also been considered [31–35].

In the case of weak anchoring on both substrates it follows from equation (7) that the texture is homeotropic if $D<D_{\mathrm{cr}}$ and distorted if $D>D_{\mathrm{cr}}$, where now

$$D_{\mathrm{cr}}=\left|\tilde{b}_0^{(\mathrm{eff})}\right|-b_D^{(\mathrm{eff})}. \quad (8)$$

Formula (8) can also be applied when the lower substrate favours a non-uniform tilted (NT) texture instead of the $U_{\pi/2}$ texture. Indeed, to determine D_{cr} we need to know $\gamma_0''\left(\bar{\theta}_0\right)$ at the local maximum $\bar{\theta}_0=0$ and not at the minimum $\bar{\theta}_0=\theta_{\mathrm{a}}^{(\mathrm{eff})}$. Thus, the derivation of equation (8) for $0<\theta_{\mathrm{a}}^{(\mathrm{eff})}<\pi/2$ is the same as for $\theta_{\mathrm{a}}^{(\mathrm{eff})}=\pi/2$.

In our model (figure 1) the true D_{cr} results from the direct minimization of F for samples of finite thickness, see equation (1). Nevertheless, asymptotic formula (8), which requires only information about individual substrates, should be a good approximation as long as $D_{\mathrm{cr}}\gtrsim p$. To show this, in figures 4 (*a*) and 4 (*b*) we plot the U_0–NT transition lines in the (p/b_2, D/p) plane, for a few values of the remaining model parameters. The curves obtained from the minimization of F exhibit a reentrant U_0–NT transition at small substrate separations. This transition is strictly related to the inhomogeneous structure of the substrates, which is reflected by its dependence on the shift ε. At large separations, however, the NT–U_0 transition is analogous to that observed in a HNC with two homogeneous substrates. This is supported by the fact that if $D_{\mathrm{cr}}\gtrsim p$ the latter transition is almost independent of ε, see figure 4 (*a*). We also note that the location of the transition line is then in a very good agreement with the prediction of asymptotic formula (8).

3.3. *4th order polynomial form of $\gamma_\alpha(\bar{\theta}_\alpha)$*

In this section we consider phase transitions in a HNC in a more general context. As in § 3.2, we assume the effective homogeneous substrate approximation [14] for the free energy of the sample, equation (6), but now the surface free energies do not have to correspond to the model of patterned substrates defined in § 2. Here we merely assume a simple form of the functions $\gamma_0(\bar{\theta}_0)$ and $\gamma_D(\bar{\theta}_D)$, which is a natural generalization of the Rapini–Papoular approximation; see equations (9) and (10). The consequence of this approach is that as long as we do not define the model of patterned substrates, to determine the functions γ_α, we cannot make any predictions about the structure of the LC–substrate interface. In particular, we cannot claim any longer that if the effective anchoring induced by a single substrate is homeotropic ($\theta_a^{(\mathrm{eff})}=0$) or planar ($\theta_a^{(\mathrm{eff})}=\pi/2$) the corresponding texture is necessarily uniform (the U_0 or $U_{\pi/2}$ texture), although it is true for the model defined in § 2. Therefore, in this context it is better to refer to homeotropic (H) and planar (P) textures, which may be non-uniform near the substrate, than to the U_0 and $U_{\pi/2}$ textures. We note, however, that we make this distinction only for formal reasons, as it has no practical consequences for our present considerations. This is because the effective homogeneous substrate approximation is reliable only if the cell thickness is large compared with the thickness of the surface region. But if this condition is satisfied we can have almost uniform homeotropic and planar textures except for thin non-uniform regions near the substrates. Note that the textures shown in figure 6 are denoted as the H, P and NT textures, where the NT texture type is distorted throughout the sample in order to satisfy conflicting anchoring conditions.

Since the surface free energy γ_α can deviate from the Rapini–Papoular form we assume the following generalization:

$$\gamma_0(\bar{\theta}_0)=\frac{1}{2}w_0\cos^2\bar{\theta}_0-\frac{1}{4}v_0\cos^4\bar{\theta}_0 \tag{9}$$

$$\gamma_D(\bar{\theta}_D)=\frac{1}{2}w_D\sin^2\bar{\theta}_D-\frac{1}{4}v_D\sin^4\bar{\theta}_D\,. \tag{10}$$

We choose $w_\alpha>0$ and $v_\alpha<w_\alpha$, which ensures that $\bar{\theta}_\alpha=0[\pi/2]$ is the minimum [maximum] of γ_D and the maximum [minimum] of γ_0, and that there are no other minima or maxima ($v_\alpha<w_\alpha<0$ would lead to a minimum at an intermediate value $0<\bar{\theta}_\alpha<\pi/2$). Then $(\gamma''_\alpha)_{\min}=w_\alpha$ and $(\gamma''_\alpha)_{\max}=-w_\alpha+v_\alpha$. For the homeotropic and planar texture the free energy reduces to

$$\begin{aligned}F_H&=F(0,0)=w_0/2-v_0/4 \text{ and}\\ F_P&=F(\pi/2,\pi/2)=w_D/2-v_D/4\end{aligned} \tag{11}$$

respectively. The homeotropic [planar] texture corresponds to a local minimum of F if $D<D_{\mathrm{cr}}^{(\mathrm{H})}\left[D<D_{\mathrm{cr}}^{(\mathrm{P})}\right]$, where

$$\frac{D_{\mathrm{cr}}^{(\mathrm{H})}}{K}=-\frac{1}{\gamma''_0(0)}-\frac{1}{\gamma''_D(0)}=\frac{1}{w_0-v_0}-\frac{1}{w_D} \tag{12}$$

$$\frac{D_{\mathrm{cr}}^{(\mathrm{P})}}{K}=-\frac{1}{\gamma''_D(\pi/2)}-\frac{1}{\gamma''_0(\pi/2)}=\frac{1}{w_D-v_D}-\frac{1}{w_0}. \tag{13}$$

Note that both $D_{\mathrm{cr}}^{(\mathrm{H})}>0$ and $D_{\mathrm{cr}}^{(\mathrm{P})}>0$ if $v_0>0$ or $v_D>0$. For $D>\max\left(D_{\mathrm{cr}}^{(\mathrm{H})},D_{\mathrm{cr}}^{(\mathrm{P})}\right)$, both the H and P textures are unstable and the minimum in F corresponds to a distorted director field (NT type). It is also worth mentioning that not all situations resulting from equations (9) and (10) can be realized in the framework of the model defined in § 2. For instance, we have not found any set of the model parameters that would yield $v_\alpha>0$. However, another model of patterned substrates could lead to a different correspondence between the model parameters and the coefficients in equations (9) and (10). We also emphasize that in order to relate the present considerations to a model of patterned substrates it should be assumed that the critical thicknesses $D_{\mathrm{cr}}^{(\mathrm{H})}$ and $D_{\mathrm{cr}}^{(\mathrm{P})}$ are large compared with the fundamental wavelength of a surface pattern.

A standard bifurcation analysis reveals that the transition from a uniform to a non-uniform texture can be either first order or continuous, depending on the parameters w_α, v_α. Expanding γ_α up to the fourth order around $\bar{\theta}_{\min}=0$ (homeotropic texture) or $\pi/2$ (planar texture) and using the equation $\partial F/\partial\bar{\theta}_D=0$ to express $\bar{\theta}_0$ as a function of $\bar{\theta}_D$, we find that the order of the transition is determined by the sign of the coefficient of $\left(\bar{\theta}_D-\bar{\theta}_{\min}\right)^3$ term in the equation $\partial F/\partial\bar{\theta}_0=0$. This coefficient involves the second and the fourth derivative of γ_α at $\bar{\theta}_{\min}$ and is given by

$$\begin{aligned}B=&-\gamma''''_0(\bar{\theta}_{\min})\left[\gamma''_D(\bar{\theta}_{\min})/\gamma''_0(\bar{\theta}_{\min})\right]^3-\\ &\gamma''''_D(\bar{\theta}_{\min})\gamma''_0(\bar{\theta}_{\min})/\gamma''_D(\bar{\theta}_{\min}).\end{aligned} \tag{14}$$

The transition is continuous if $B>0$, first order if $B<0$, and $B=0$ corresponds to a tricritical point. Possible topologies of the phase diagram are shown in figures 6 (*a*)–(*d*). The phase diagrams are presented in the (v_D/w_D, Dw_0/K) plane (here K/w_0 serves as the length unit), for several values of w_D and v_0/w_0. In figure 6 (*a*) we observe a triple point, at which the phases H, P and

NT coexist, and one tricritical point, at which the H–NT transition changes from a first order to a continuous one. The case of one triple point and three tricritical points is shown in figure 6 (*b*). Here the P–NT transition is continuous in some interval of v_D/w_D, hence there are two tricritical points on the transition line. In figure 6 (*c*) the continuous P–NT transition line terminates at a critical end point on the first order H–NT transition line. Finally, in figure 6 (*d*) there are only two phases: P and NT, separated by a transition line with one tricritical point. We note that the presence of first order transition lines in these phase diagrams suggests the possibility of switching between two states whose energies are equal or close to each other.

4. Conclusions

We have applied the Frank–Oseen theory together with the Rapini–Papoular surface free energy to nematic liquid crystals (NLCs) confined between two substrates possessing an alternating stripe pattern of planar and homeotropic anchoring (figure 1). The total free energy is minimized numerically, and phase diagrams as well as effective anchoring strengths are determined with the following main results.

(1) Figure 2 shown that the phase transition between non-uniform tilted (NT) and uniform homeotropic (U_0) textures of a NLC confined between two identically patterned substrates can be triggered by changing the shift ε of the stripe patterns with respect to each other. The location of the U_0–NT transition, as a function of the anchoring strength, is almost independent of ε for substrate separations D larger than the periodicity of the stripe pattern p (figure 3).

(2) A stable U_0 phase can also be found in the case that one of the substrates favours a uniform planar ($U_{\pi/2}$) texture or a tilted nematic director (figure 4). The latter possibility is related to the

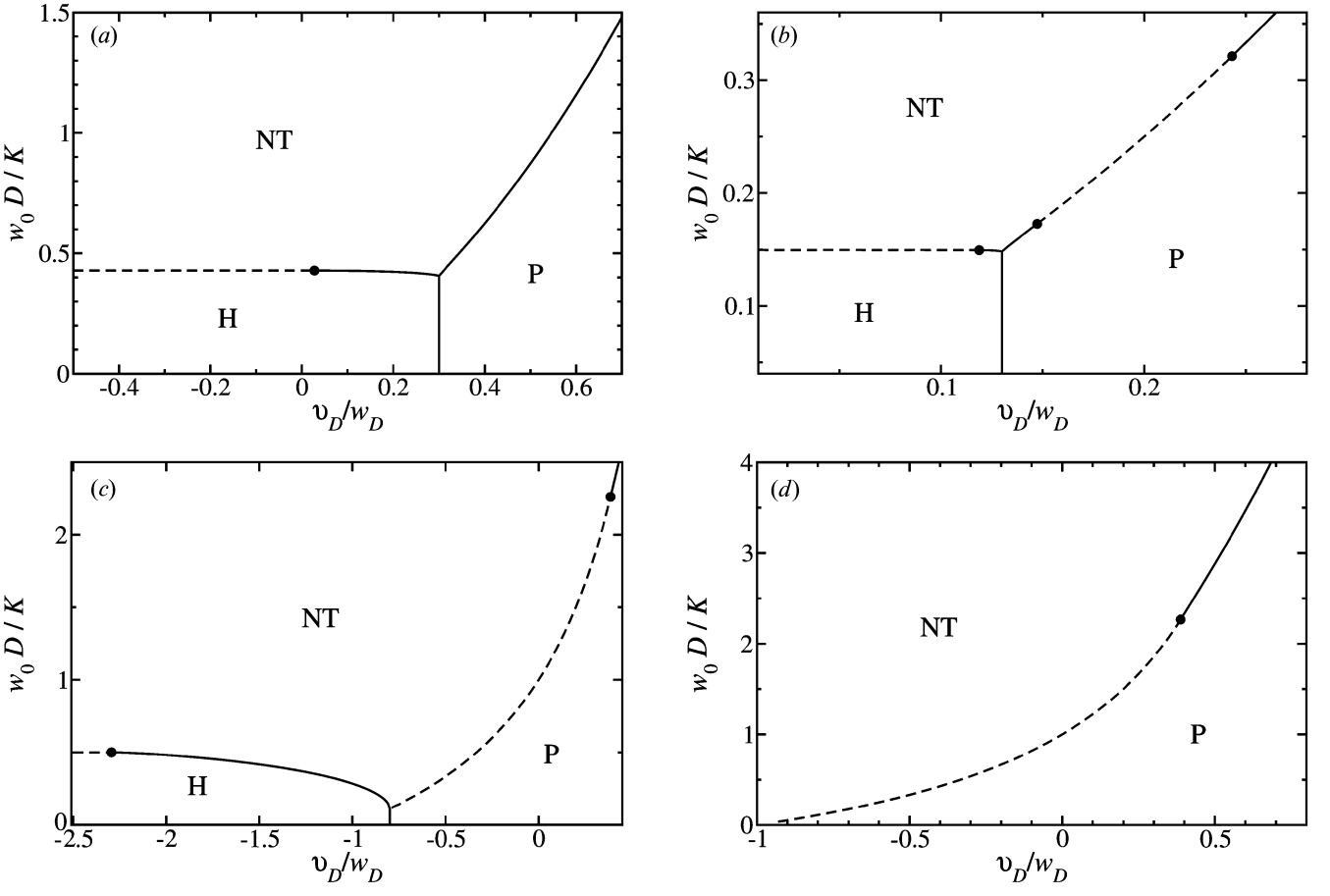

Figure 6. Phase diagrams for a HNC with two effective homogeneous substrates (see text): the lower substrate favours the homeotropic (H) texture and the upper favours the planar (P) texture. The anchoring energy functions are given by equations (9) and (10) with $w_D/w_0=1$, $v_0/w_0=0.3$ in (*a*); $w_D/w_0=1$, $v_0/w_0=0.13$ in (*b*); $w_D/w_0=0.5$, $v_0/w_0=0.6$ in (*c*); $w_D/w_0=0.5$, $v_0/w_0=0.5$ in (*d*). The solid and dashed lines show first order and continuous transitions, respectively, and the black circles mark the tricritical points.

fact that in our model the surface free energy of the interface between the NLC and the effective homogeneous substrate, γ_α, deviates from the Rapini–Papoular form.

(3) The effective anchoring strength of a single periodically patterned and flat substrate vanishes at U_0–NT and $U_{\pi/2}$–NT phase transitions (figure 5). Using this effective anchoring strength, a hybrid nematic cell (HNC) model can be used to describe the phase behaviour of the confined NLC for substrate separations D larger than the periodicity of the stripe pattern p (figure 4).

(4) Rich phase diagrams, involving the NT, homeotropic (H) and planar (P) textures are found for a HNC with a 4th order polynominal form for the surface free energy (figure 6). The transitions between the phases can be either first or second order.

Finally, it would be interesting to consider the effect of surface roughness, superimposed on the stripe pattern, on the phase transition between a uniform and a non-uniform texture. We defer this study to a future work.

Acknowledgement

This work was partially supported by the KBN grant No. 5P03B01121.

References

[1] P.G. De Gennes, J. Prost. *The Physics of Liquid Crystals*. 2nd Edn, Clarendon Press, Oxford (1993).
[2] B. Jérôme. *Rep. Prog. Phys.*, **54**, 391 (1991).
[3] B. Jérôme, P. Pieranski, M. Boix. *Europhys. Lett.*, **5**, 693 (1988).
[4] M. Monkade, M. Boix, G. Durand. *Europhys. Lett.*, **5**, 697 (1988).
[5] R. Barberi, M. Giocondo, M. Iovane, I. Dozov, E. Polossat. *Liq. Cryst.*, **25**, 23 (1998).
[6] P. Jägemalm, L. Komitov, G. Barbero. *Appl. Phys. Lett.*, **73**, 1616 (1998).
[7] P. Jägemalm, G. Barbero, L. Komitov, A.K. Zvezdin. *Phys. Rev. E*, **58**, 5982 (1998).
[8] G. Barbero, P. Jägemalm, A.K. Zvezdin. *Phys. Rev. E*, **64**, 021703 (2001).
[9] C.V. Brown, M.J. Towler, V.C. Hui, G.P. Bryan-Brown. *Liq. Cryst.*, **27**, 233 (2000).
[10] C. Denniston, J.M. Yeomans. *Phys. Rev. Lett.*, **87**, 275505 (2001).
[11] D.W. Berreman. *Phys. Rev. Lett.*, **28**, 1683 (1972).
[12] S. Faetti. *Phys. Rev. A*, **36**, 408 (1987).
[13] H.L. Ong, A.J. Hurd, R.B. Meyer. *J. appl. Phys.*, **57**, 186 (1985).
[14] G. Barbero, T. Beica, A.L. Alexe-Ionescu, R. Moldovan. *J. Phys. II Fr.*, **2**, 2011 (1992).
[15] T.Z. Qian, P. Sheng. *Phys. Rev. Lett.*, **77**, 4564 (1996).
[16] T.Z. Qian, P. Sheng. *Phys. Rev. E*, **55**, 7111 (1997).
[17] V.K. Gupta, N.L. Abbott. *Science*, **276**, 1533 (1997).
[18] B.-W. Lee, N.A. Clark. *Science*, **291**, 2576 (2001).
[19] P. Patrício, M.M. Telo da Gama, S. Dietrich. *Phys. Rev. Lett.*, **88**, 245502 (2002).
[20] H.T.A. Wilderbeek, F.J.A. van der Meer, K. Feldmann, D.J. Broer, C.W.M. Bastiaansen. *Adv. Mater.*, **14**, 655 (2002).
[21] H.T.A. Wilderbeek,J.-P. Teunissen,C.W.M. Bastiaansen, D.J. Broer. *Adv. Mater.*, **15**, 985 (2003).
[22] F.C. Frank. *Discuss. Faraday Soc.*, **25**, 19 (1958).
[23] A. Rapini, M. Papoular. *J. Phys. (Paris) Colloq.*, **30**, C4–54 (1969).
[24] S. Kondrat, A. Poniewierski. *Phys. Rev. E*, **64**, 031709 (2001).
[25] S. Kondrat, A. Poniewierski, L. Harnau. *Eur. Phys. J. E*, **10**, 163 (2003).
[26] E. Dubois-Violette, P.G. de Gennes. *J. colloid interface Sci.*, **57**, 403 (1976).
[27] A. Poniewierski, A. Samborski. *Liq. Cryst.*, **23**, 377 (1997).
[28] G. Barbero, R. Barberi. *J. Physique*, **44**, 609 (1983).
[29] B. Wen, C. Rosenblatt. *Phys. Rev. Lett.*, **89**, 195505 (2002).
[30] A. Šarlah, S. Žumer. *Phys. Rev. E*, **60**, 1821 (1999).
[31] H. Yokoyama, H.A. van Sprang. *J. appl. Phys.*, **57**, 4520 (1985).
[32] T.J. Sluckin, A. Poniewierski. *Fluid Interfacial Phenomena*, C.A. Croxton (Ed.), Chap. 5, Wiley, Chichester (1986).
[33] G. Barbero, Z. Gabbasova, Y.A. Kosevich. *J. Phys. II Fr.*, **1**, 1505 (1991).
[34] A.L. Alexe-Ionescu, G. Barbero, Z. Gabbasova, G. Sayko, A.K. Zvezdin. *Phys. Rev. E*, **49**, 5354 (1994).
[35] J.-B. Fournier, P. Galatola. *Phys. Rev. Lett.*, **82**, 4859 (1999).

Appendix

Discretization of the free energy

For our purpose it suffices to discretize $\theta(x, z)$ only in the x direction. Thus, we introduce $N+1$ functions: $\vartheta_n(z)=\theta(x_n, z)$, where $x_n=hn$ for $n=0, \ldots, N$, $h=p/N$ and $\vartheta_0(z)=\vartheta_N(z)$ (periodic boundary conditions). Then F is given by (for simplicity we use the same symbols for the discrete and continuous case)

$$F[\{\vartheta_n\}, N]=\frac{Kh}{2}\sum_{n=0}^{N-1}\int_0^D \mathrm{d}z\left\{\left[\frac{\vartheta_{n+1}(z)-\vartheta_n(z)}{h}\right]^2+\left(\frac{\mathrm{d}\vartheta_n}{\mathrm{d}z}\right)^2\right\}+\frac{h}{2}\sum_{n=0}^{N-1}\left(w_n^{(0)}\sin^2\vartheta_n^{(0)}+w_n^{(D)}\sin^2\vartheta_n^{(D)}\right) \quad \text{(A1)}$$

where $w_n^{(\alpha)}=w_\alpha(x_n)$, $\vartheta_n^{(\alpha)}=\theta_\alpha(x_n)$, and $\alpha=0$, D. Minimization with respect to $\vartheta_0(z)$, …, $\vartheta_{N-1}(z)$ at fixed boundary conditions at $z=0$ and $z=D$ leads to the following set of N equations

$$h^{-2}(\vartheta_{n+1}-2\vartheta_n+\vartheta_{n-1})+\frac{\mathrm{d}^2\vartheta_n}{\mathrm{d}z^2}=0. \quad \text{(A2)}$$

A general solution of equation (A2) has the form of a discrete Fourier transform

$$\vartheta_n(z) = A_0 + (B_0 - A_0)\frac{z}{D} + \sum_{l=1}^{N-1} \exp(2\pi i n l/N)\left\{\frac{A_l \sinh[k_l(D-z)]}{\sinh(k_l D)} + B_l \frac{\sinh(k_l z)}{\sinh(k_l D)}\right\} \tag{A3}$$

with wave vectors $k_l = 2h^{-1}\sin(\pi l/N)$. The coefficients A_l and B_l are related to the boundary functions $\vartheta_n^{(\alpha)}$ via the inverse discrete Fourier transforms:

$$A_l = \frac{1}{N}\sum_{n=0}^{N-1} \vartheta_n^{(0)} \exp(-2\pi i l n/N)$$
$$B_l = \frac{1}{N}\sum_{n=0}^{N-1} \vartheta_n^{(D)} \exp(-2\pi i l n/N). \tag{A4}$$

Since $\vartheta_n^{(0)}$ and $\vartheta_n^{(D)}$ are real we have for the complex conjugates $A_l^* = A_{N-l}$ and $B_l^* = B_{N-1}$. A_0 and B_0 are the average director orientations (averaged over the period p) at the two limiting surfaces. Substituting equation (A3) into (A1) we obtain F_d in terms of the Fourier components:

$$F_\mathrm{d}(\{A_l\}, \{B_l\}, N) = \frac{Kp}{2}\left[\frac{(B_0 - A_0)^2}{D} + \sum_{l=1}^{N-1} k_l \coth(k_l D)\left(|A_l|^2 + |B_l|^2\right) - \sum_{l=1}^{N-1} k_l \sinh^{-1}(k_l D)\left(A_l B_l^* + A_l^* B_l\right)\right] \tag{A5}$$

and because of equation (A4) F_d can also be considered as a function of $2N$ independent surface variables $\vartheta_n^{(0)}$ and $\vartheta_n^{(D)}$. This is actually more convenient than expressing F_d in terms of Fourier components. Thus, we have

$$F_\mathrm{d}\left(\left\{\vartheta_n^{(0)}\right\}, \left\{\vartheta_n^{(D)}\right\}, N\right) = \frac{Kp}{2}\left[\frac{(B_0 - A_0)^2}{D} + \frac{1}{N^2}\sum_{n=0}^{N-1}\sum_{n'=0}^{N-1} V_{00}(n-n', N) \times \left(\vartheta_n^{(0)}\vartheta_{n'}^{(0)} + \vartheta_n^{(D)}\vartheta_{n'}^{(D)}\right) - \frac{2}{N^2}\sum_{n=0}^{N-1}\sum_{n'=0}^{N-1} V_{0D}(n-n', N)\vartheta_n^{(0)}\vartheta_{n'}^{(D)}\right] \tag{A6}$$

where (for odd N)

$$V_{00}(m, N) = V_{DD}(m, N) = \sum_{l=1}^{N-1} k_l \coth(k_l D)\cos(2\pi m l/N) \tag{A7}$$

$$V_{0D}(m, N) = V_{D0}(m, N) = \sum_{l=1}^{N-1} k_l \sinh^{-1}(k_l D)\cos(2\pi m l/N). \tag{A8}$$

Semi-infinite system

The distortion free energy for a semi-infinite system, which we denote by $F_\mathrm{d}^{(\infty)}$, can be obtained directly from expression (A6) by taking the limit $D\to\infty$ and $\vartheta_n^{(D)} = 0$:

$$F_\mathrm{d}^{(\infty)}\left(\left\{\vartheta_n^{(0)}\right\}, N\right) = \frac{Kp}{2N^2}\sum_{n=0}^{N-1}\sum_{n'=0}^{N-1} V_{00}^{(\infty)}(n-n')\vartheta_n^{(0)}\vartheta_{n'}^{(0)}. \tag{A9}$$

In this special case the limit $V_{00}^{(\infty)}(m) = \lim_{D\to\infty} V_{00}(m)$ can be calculated analytically:

$$V_{00}^{(\infty)}(m, N) = \sum_{l=1}^{N-1} k_l \cos(2\pi m l/N) = -\frac{(N/p)\sin(\pi/N)}{\sin^2(\pi m/N) - \sin^2(\pi/2N)}. \tag{A10}$$

Making use of the identity $\sum_{n=0}^{N-1} V_{00}(n-n') = 0$ and assuming that π/N is small we find

$$F_\mathrm{d}^{(\infty)}\left(\left\{\vartheta_n^{(0)}\right\}, N\right) = \frac{\pi K}{4p^2}h^2 \sum_{n=0}^{N-1}\sum_{n'=0}^{N-1} \frac{\left(\vartheta_n^{(0)} - \vartheta_{n'}^{(0)}\right)^2}{\sin^2[\pi(n-n')/N] - (\pi/2N)^2} \tag{A11}$$

which in the limit of $N\to\infty$ tends to

$$\lim_{N\to\infty} F_\mathrm{d}^{(\infty)}(\{\vartheta_n^0\}, N) = \frac{\pi K}{4p^2}\int_0^p \mathrm{d}x \int_0^p \mathrm{d}x' \frac{[\theta_0(x) - \theta_0(x')]^2}{\sin^2[\pi(x-x')/p]}. \tag{A12}$$

Thus, we have recovered the function $F_\mathrm{d}[\theta_0]$ for the continuous case, derived previously by means of the Green's function method [24]. We note that a slightly different discrete expression for $F_\mathrm{d}^{(\infty)}$ has been obtained in [24] because it has been derived directly from the continuous expression (A12). However, we have checked numerically that this difference is negligible provided N is sufficiently large.

Determination of $b^{(eff)}$

To find the effective extrapolation length we express the function $\psi(x, z)$, see equation (5), in terms of a discrete Fourier series

$$\psi_n(z)=\psi(x_n, z)=\sum_{l=0}^{N-1} A_l \exp(2\pi i n l/N)\exp(-k_l z) \quad \text{(A13)}$$

where

$$Al=\frac{1}{N}\sum_{n=0}^{N-1}\psi_n^{(0)}\exp(-2\pi i l n/N) \quad \text{(A14)}$$

and $\psi_n^{(0)}=\psi_n(0)$. Hence $\psi_n(z)$ satisfies equation (A2) and the boundary condition $d\psi_n(z)/dz=0$ at $z=\infty$. From equations (5), (A13) and (A14) we find

$$1-\frac{1}{N}\sum_{n'=0}^{N-1} V_{00}^{(\infty)}(n-n', N)\psi_{n'}^{(0)} = K^{-1}w_n^{(0)}\cos\left[2\theta_0^{(\infty)}(x_n)\right]\psi_n^{(0)}. \quad \text{(A15)}$$

Note that $b^{(\mathrm{eff})}=A_0=\sum_{n=0}^{N-1}\psi_n^{(0)}\Big/N$.